J. Fluid Mech. (1996), vol. 321, pp. 217–233

Subharmonic resonance of short internal standing waves by progressive surface waves

By D. F. HILL AND M. A. FODA

Environmental Water Resources, Department of Civil Engineering,
University of California at Berkeley, Berkeley, CA 94720, USA

(Received 18 December 1995 and in revised form 1 April 1996)

Experimental evidence and a theoretical formulation describing the interaction between a progressive surface wave and a nearly standing subharmonic internal wave in a two-layer system are presented. Laboratory investigations into the dynamics of an interface between water and a fluidized sediment bed reveal that progressive surface waves can excite short standing waves at this interface. The corresponding theoretical analysis is second order and specifically considers the case where the internal wave, composed of two oppositely travelling harmonics, is much shorter than the surface wave. Furthermore, the analysis is limited to the case where the internal waves are small, so that only the initial growth is described. Approximate solution to the nonlinear boundary value problem is facilitated through a perturbation expansion in surface wave steepness. When certain resonance conditions are imposed, quadratic interactions between any two of the harmonics are in phase with the third, yielding a resonant triad. At the second order, evolution equations are derived for the internal wave amplitudes. Solution of these equations in the inviscid limit reveals that, at this order, the growth rates for the internal waves are purely imaginary. The introduction of viscosity into the analysis has the effect of modifying the evolution equations so that the growth rates are complex. As a result, the amplitudes of the internal waves are found to grow exponentially in time. Physically, the viscosity has the effect of adjusting the phase of the pressure so that there is net work done on the internal waves. The growth rates are, in addition, shown to be functions of the density ratio of the two fluids, the fluid layer depths, and the surface wave conditions.

1. Introduction

The present work is motivated by recent studies on wave–seabed interactions. It is well known that the loading of water waves on a sediment bed can result in bulk fluidization of the bed. This refers to the condition in which the contact stresses between particles vanish and results in the bed losing its shear strength and behaving much like a fluid. The broad-based interest in understanding this phenomenon derives from its application to studies in sediment transport, wave attenuation, and the design of marine structures.

Recent experimental efforts by Foda & Tzang (1994) reported that under the loading of progressive surface waves, a silty sediment bed was repeatedly and extensively fluidized. The present study details further experiments, as well as a theoretical formulation, which specifically address the issue of the behaviour of the water–sediment interface following fluidization. The experimental results demonstrate the formation

of short, standing, subharmonic waves at the interface. The objective of the theoretical analysis, therefore, is to provide a description of a general mechanism for subharmonic resonance of internal waves by a progressive surface wave. The specific focus is on the case where the internal waves are much shorter than the generating surface wave. By assuming the fluidized sediment bed to be a fluid, one major difficulty is immediately surmounted and the analysis reduces to one of pure fluid mechanics.

Numerous previous studies have addressed the topic of interactions between surface and internal waves. A linear resonance theory by Ting & Raichlen (1986) describes the generation of internal waves inside a trench of finite length. In this analysis, internal waves were found to be excited when the frequency of the overlying surface wave matched the frequency of one of the internal wave modes of the trench. To describe the excitation of non-synchronous internal waves, however, clearly requires a nonlinear theory.

Ball (1964) was the first to propose nonlinear resonant excitation of internal waves by surface waves and went on to demonstrate that interactions between surface waves and internal waves could take place at the second order. Specifically, he employed the nonlinear shallow water equations in order to present a wave-triad resonance theory between two oppositely travelling surface waves and a progressive internal wave. Absent from Ball's theory were the effects of wave dispersion and fluid viscosity. Dispersion effects were later considered by Brekhovskikh *et al.* (1972) and Thorpe (1966) in attempts to extend Ball's theory for the same interacting triad.

When the waves satisfied a resonance condition, it was shown that initial growth of the internal wave was linear in time. Mathematically, this condition corresponds to

$$\bar{\lambda} = \bar{k}_1 - \bar{k}_2$$
$$\sigma = \omega_1 - \omega_2$$

where σ and $\bar{\lambda}$ are the internal wave's frequency and wavenumber vector, and ω_i and $\bar{k}_i$, i=1,2 are the frequencies and wavenumber vectors corresponding to the surface waves.

This triad is graphically illustrated in figure 1(*a*), which shows the dispersion relationship of a two-layer fluid system with a free surface and layers of finite depth. The different branches of the curve represent both surface and internal waves, denoted by S and I respectively, and right- and left-travelling waves, denoted by 1 and 2. An arbitrary wave may be represented as a vector originating at the origin and terminating on one of the branches of the curve. From the principles of vector addition, a resonant triad is therefore defined by any three wave vectors which make up the sides and diagonal of a parallelogram. Ball demonstrated that, associated with the arbitrary surface wave denoted by point A, there were two possible triads. These triads are denoted by the points A, B1 and C1 and A, B2 and C2 respectively.

The present study seeks to further extend the interaction problem by looking at a different interaction path, with a wave triad different from that considered by previous authors. The primary carrier of energy is a single progressive surface wave with amplitude of order unity. Two oppositely travelling small internal wave perturbations complete the triad. The viability of this triad is clearly illustrated in figure 1(*b*). The points A, B3 and C3 represent a third resonant triad involving the same arbitrary surface wave considered by Ball. Moreover, it is clear that the internal waves are quite short in comparison to the surface wave and are very nearly subharmonic to the surface wave.

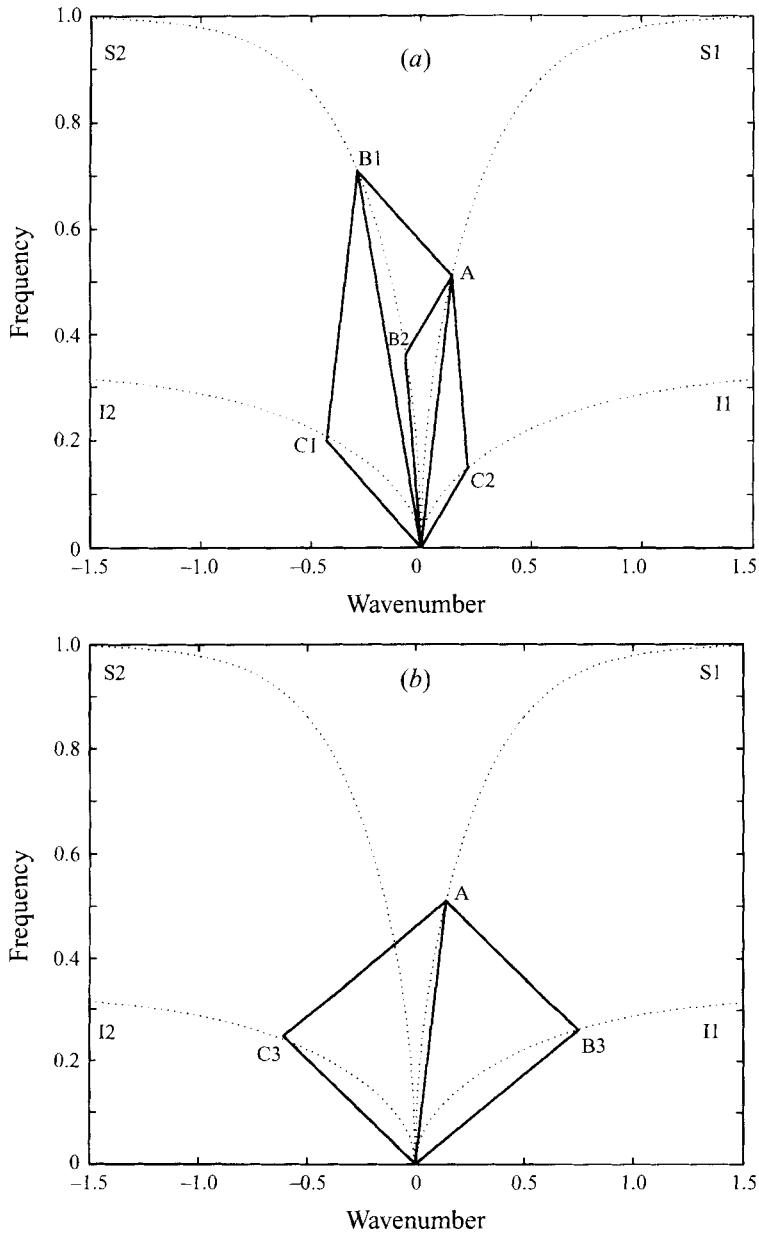

FIGURE 1. Two-layer dispersion relationship: (*a*) illustrating resonant triads pursued by Ball (1964), (*b*) illustrating new resonant triad.

The present analysis uses both a perturbation expansion of the velocity potential and a multiple time scale, in which the internal wave amplitudes are assumed to be slowly varying functions of time. Only the two-dimensional problem, in which all three waves are plane and parallel, is considered. Dispersion effects are included by allowing for variable fluid depths. The analysis proceeds by first developing the leading-order linear harmonic solutions for the surface and internal waves. At the second order, quadratic interactions among the linear harmonics provide the forcing for the higher-order harmonics. A solvability condition, in the form of an

application of Green's theorem, is then imposed on the inhomogeneous second-order problem. This condition yields the desired evolution equations for the internal wave perturbations.

In addition to pursuing an entirely new triad, the present analysis differs fundamentally from those of the previous authors in that a single wave is the primary carrier of energy. The difference emerges upon consideration of the general interaction equations. For a wave triad in a general system with no dissipation, the interaction equations are given by (see e. g. Simmons 1969)

$$\frac{da_1}{dt_1} = i\alpha_1 a_2 a_3, \quad \frac{da_2}{dt_1} = i\alpha_2 a_1 a_3^*, \quad \frac{da_3}{dt_1} = i\alpha_3 a_1 a_2^*.$$

In the above, a_1, a_2, and a_3 are the complex amplitudes, which are functions of the slow time scale t_1. The interaction coefficients α_1, α_2, and α_3 are specific to the particular system being considered. The nature of this set of equations is such that if all three of the amplitudes are assumed to be of the same order, say $O(1)$, then the solutions are elliptic functions of time. If two of the amplitudes, say a_1 and a_2, are assumed to be $O(1)$ and a_3 is assumed to be $O(\epsilon)$, then, to the leading order, only the third equation is retained and a_3 will initially grow linearly in time. As a_3 becomes $O(1)$, the other two equations will become significant and the three harmonics will continue to exchange energy. These are the results found by Ball.

In the present analysis, however, a_3 is defined as the surface wave amplitude, assumed to be $O(1)$, and a_1 and a_2 are defined as the internal wave amplitudes, each assumed to be $O(\epsilon)$. The slow time derivatives of the internal wave amplitudes are therefore $O(1)$, and that of the surface wave $O(\epsilon^2)$. To the leading order of analysis, therefore, the third equation is discarded. Solution of the two remaining equations reveals that the internal wave amplitudes evolve exponentially with growth rates $\pm(-\alpha_1\alpha_2)^{1/2}$. These growth rates are consequently shown to be purely imaginary. In other words, despite the presence of a resonant triad, there is no growth at this order of analysis.

Following the inviscid formulation, which leads to a marginally stable interaction, viscosity is introduced for the first time into the general interaction problem. The results indicate that viscosity triggers an exponential growth of the internal wave amplitudes. Mathematically, the inclusion of the viscous terms modifies the coefficients of the evolution equations so that the growth rates are complex rather than purely imaginary. From a physical standpoint, the inclusion of viscosity adjusts the phase of the pressure forcing the internal wave so that there is net work done over a wave period. This role of viscosity as a destabilizing rather than a stabilizing agent has emerged as a significant and unexpected result of the present analysis.

2. Experimental investigation

2.1. *Setup*

The experiments were conducted in a wave flume measuring 30 m in length, 1.86 m in depth and 0.45 m in width. Surface waves were generated at one end by a hinged mechanical wavemaker and absorbed at the other end by a 1:10 slope beach. A false floor was constructed so as to create a sediment trench 3.0 m in length, 0.85 m in depth and 0.45 m in width. A 1:8 slope ramp was used to provide smooth transition in bottom depth. The details of the experimental setup can be seen in figure (2).

The first step in the experimental procedure consisted of placing the sediment bed in the trench. The soil used was a commercially available fine silt with a mean grain

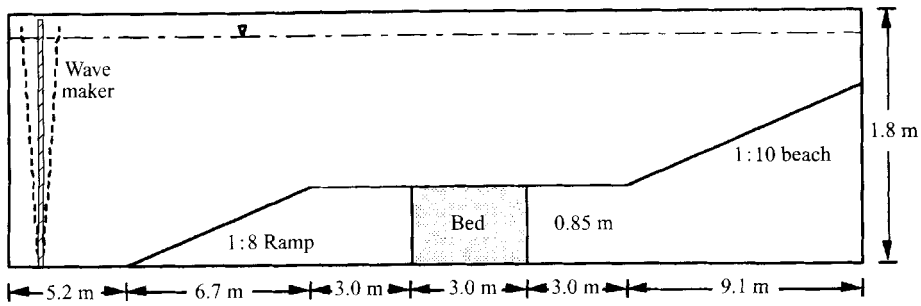

FIGURE 2. Experimental setup.

size of $d_{50} = 50$ μm. The bed was placed by partitioning off the trench from the rest of the flume and filling it with a well-mixed slurry of soil and water. This was then allowed to settle overnight. The partitions were then removed and the flume slowly filled with water. A typical experimental run consisted of a period of wave loading of the order of three minutes. After a run, the bed was allowed to reconsolidate for a period of the order of half a day. In this way, successive experiments could be conducted on the same bed without remixing, allowing investigation into the effects of cyclic fluidization and consolidation.

The interface between the water and the sediment bed was recorded using a Panasonic video camera, operating at thirty frames per second. Two incandescent lamps affixed to the top of the flume served to illuminate the region over the bed. Graphic images were acquired using a Data Translation DT2851 Image Grabber and IPPLUS image processing software. To obtain qualitative results required only some adjustment of contrast and minor editing.

2.2. *Results*

Figure 3 details a series of images of the water–sediment interface. For this experimental run, surface waves having a period of $T = 1.4$ s were generated in water of 0.60 m depth. Note that this depth refers to the false floor and not the actual floor of the flume. The amplitude of the surface wave was 0.14 m, and the wavelength over the bed was roughly 2.7 m.

The images are spaced at $0.5T$ intervals, and clearly show a flat interface alternating with one characterized by distinct, regular ripples. For example, the image at $3.0T$ shows three prominent crests and two troughs. The following image at $3.5T$ shows a flat interface. At $4T$, three troughs and two crests are seen which are very nearly 180° out of phase with those seen at $3T$. This pattern persists in the next few images so that the image at $5T$ is virtually identical to that at $3T$, with a slight phase shift.

This, combined with the fact that the period of this behaviour is $2T$ demonstrates the presence of a nearly standing wave that is subharmonic to the surface wave. Moreover, the wavelength of the ripples in the images is approximately 0.3 m, a full order of magnitude shorter that the surface wave. These experimental results therefore strongly motivate the pursuit of a theoretical formulation of this wave-triad interaction.

3. Theoretical formulation

The origin of a two-dimensional Cartesian coordinate system is placed on the undisturbed interface between a surface layer of depth H, density ρ, and viscosity

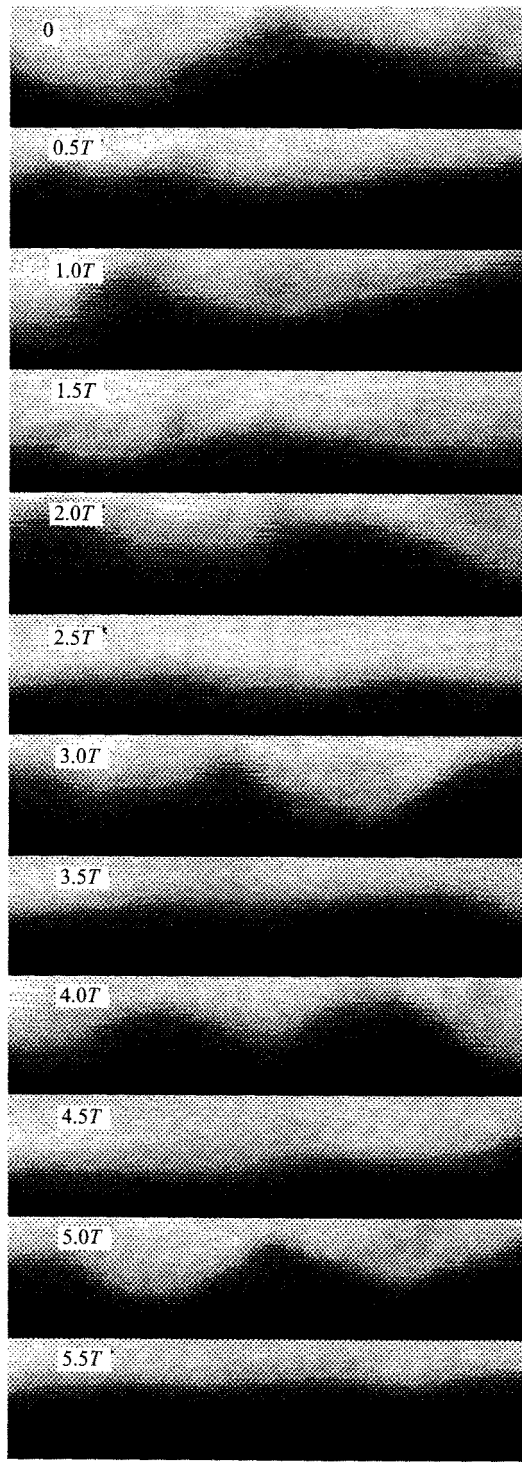

FIGURE 3. Images of water-sediment interface. Images are at intervals of one half of the surface wave period.

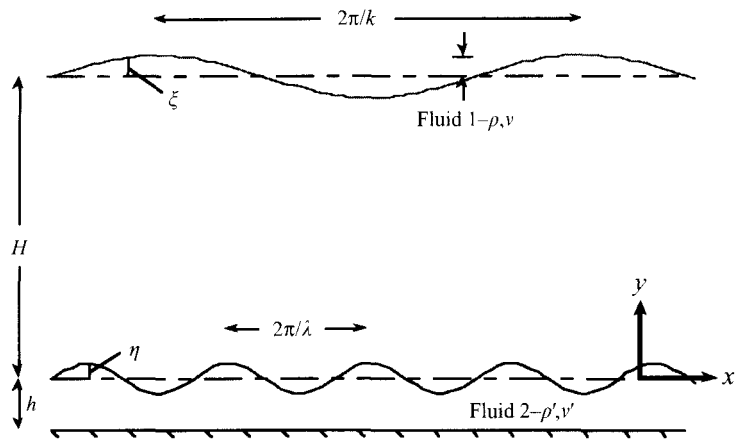

FIGURE 4. Adopted configuration.

ν, and a viscous lower layer of depth h, density ρ', and viscosity ν', as sketched in figure 4. The y-coordinate is defined as pointing vertically upward and the density ratio $\gamma = \rho/\rho'$ is assumed to be less than unity. To the leading order, the wave field is made up of a linear progressive surface wave of amplitude A, wavenumber k, and frequency ω, propagating in the positive x-direction. The perturbation internal waves have amplitudes a_1 and a_2, wavenumbers λ_1 and λ_2, frequencies σ_1 and σ_2, and propagate in the negative and positive x-directions, respectively. Note that a_1, a_2 and A are taken to be complex and λ_1, λ_2, σ_1, and σ_2 are all defined to have positive real values. For resonant interactions to occur, the following resonance conditions are imposed on the triad's wavenumbers and frequencies:

$$\lambda_2 - \lambda_1 = k, \tag{1}$$

$$\sigma_1 + \sigma_2 = \omega. \tag{2}$$

From the assumption that the wavenumber of the surface wave is much smaller than the wavenumbers of the internal waves, (1) implies that $\lambda_1 \approx \lambda_2$. From the dispersion relationships of the internal waves, this can be seen to result in $\sigma_1 \approx \sigma_2$. From (2), it can then be concluded that $\sigma_1, \sigma_2 \approx \frac{1}{2}\omega$. In other words, the internal waves are each nearly subharmonic to the surface wave and, as such, comprise a nearly standing wave, as was illustrated in figure 2. With this established, attention is turned to the mathematical formulation of the problem.

In both layers, the Navier–Stokes equations are employed:

$$\nabla \cdot \boldsymbol{u} = 0, \qquad -h \leqslant y \leqslant H + \xi, \tag{3}$$

$$\frac{\mathrm{D}\boldsymbol{u}}{\mathrm{D}t} = -\nabla\left(\frac{p}{\rho} + gy\right) + \nu\nabla^2\boldsymbol{u}, \qquad 0 \leqslant y \leqslant H + \xi, \tag{4}$$

$$\frac{\mathrm{D}\boldsymbol{u}}{\mathrm{D}t} = -\nabla\left(\frac{p}{\rho'} + gy\right) + \nu'\nabla^2\boldsymbol{u}, \qquad -h \leqslant y \leqslant 0, \tag{5}$$

where $\boldsymbol{u} = (u, v)$ is the velocity vector, g is the acceleration due to gravity, and p is the pressure.

The kinematic and dynamic free-surface boundary conditions are given by

$$\frac{D\xi}{Dt} = v, \qquad y = H + \xi, \tag{6}$$

$$p = 0, \qquad y = H + \xi, \tag{7}$$

In the above, ξ is the free-surface displacement from its equilibrium value of H.

At the bottom of the lower layer, the following no-slip and no-flow conditions are imposed:

$$u = 0, \qquad y = -h, \tag{8}$$

$$v = 0, \qquad y = -h. \tag{9}$$

At the perturbed interface between the two liquids, the usual kinematic conditions are given by

$$\eta_t + u^+\eta_x = v^+, \qquad y = \eta, \tag{10}$$

$$\eta_t + u^-\eta_x = v^-, \qquad y = \eta, \tag{11}$$

where η is the displacement of the interface from its equilibrium value of $y = 0$. The + and − superscripts denote evaluation of the velocities at $y = \eta^+$ and $y = \eta^-$ respectively.

The dynamic condition of continuity of normal stress at the interface requires

$$(p - 2\rho v v_y)^+ = (p - 2\rho' v' v_y)^-, \qquad y = \eta. \tag{12}$$

And finally, owing to the inclusion of viscosity in both layers, there are the additional conditions of continuity of shear stress and horizontal velocity:

$$\rho v(u_y + v_x)^+ = \rho' v'(u_y + v_x)^-, \qquad y = \eta, \tag{13}$$

$$u^+ = u^-, \qquad y = \eta. \tag{14}$$

4. Solution

Equations (3)–(14) define the adopted model for the coupled two-layer system. A perturbation analysis is subsequently employed to facilitate approximate solution to the above equations. The analysis is carried to the second order of interaction, and as a first step, the following choices of non-dimensionalization are introduced:

$$(x^*, y^*) = k(x, y), \qquad t^* = (gk)^{1/2}t, \qquad H^* = kH,$$

$$(\omega^*, \sigma_1^*, \sigma_2^*) = \frac{(\omega, \sigma_1, \sigma_2)}{(gk)^{1/2}}, \qquad \xi^* = \frac{\xi}{A}, \qquad \eta^* = \frac{\eta}{kA^2},$$

$$h^* = \lambda_1 h, \qquad (u^*, v^*) = \frac{(u, v)}{A(gk)^{1/2}}, \qquad \Phi^* = \frac{\Phi}{A(g/k)^{1/2}},$$

$$p^* = \frac{p}{\rho' gA}, \qquad (v^*, v'^*) = \frac{(v, v')k^2}{(gk)^{1/2}}, \qquad (a_1, a_2) = \frac{(a_1, a_2)}{kA^2}.$$

In the above equations, A is the constant amplitude of the surface wave, and the asterisks denote non-dimensional quantities. Substitution of these variables into the governing equations reduces the solution to a purely non-dimensional one and the asterisks will be dropped for convenience.

Next, several small parameters are identified. The first is the steepness of the surface wave, denoted as

$$\epsilon = kA.$$

Additionally, it is desirable to introduce new viscosity parameters, scaled as

$$\nu' = \epsilon^4 \kappa', \quad \nu = \epsilon^6 \kappa, \quad \frac{\nu}{\nu'} = O(\epsilon^2),$$

where κ and κ' can be up to $O(1)$. These particular choices of scaling may seem arbitrary, but they in fact serve two very significant purposes. First, the assumption of relatively weak viscosity in both layers removes to the third order some of the viscous effects. This will be discussed in greater detail later. Second, the assumption that the upper fluid be much less viscous than the lower fluid allows a reduction of the interfacial boundary conditions. This is physically consistent with the situation of having a layer of water over a layer of fluidized sediment. As a consequence, (13) can be shown to reduce to the following form:

$$(u_y + v_x)^- = O(\epsilon), \qquad y = \eta. \tag{15}$$

In other words, the condition of continuity of interfacial shear reduces, to the leading order, to the condition that the shear in the lower layer is zero at the interface. This reduces the problem to one of an inviscid upper layer overlying a viscous lower layer.

Finally, and as previously mentioned, the wavelengths of the internal waves are assumed much smaller than that of the surface wave, yielding two more small parameters of the form

$$\epsilon \ll \mu_i = \frac{k}{\lambda_i} \ll 1, \qquad i = 1, 2.$$

It is worth noting that it is possible to proceed without this last assumption and devise an analysis for a general wave triad. However, the laboratory observations motivate concentration on short internal waves. Additionally, unless $\mu_i, i = 1, 2$ are small, it is not possible to obtain nearly subharmonic behaviour at the interface. The relative scalings between ϵ and μ_i are essential to the convergence of the problem.

In the lower layer, it is desirable to isolate the effect of viscosity. To this end, the velocity vector $\boldsymbol{u}$ may be taken as the sum of an inviscid irrotational vector (Φ_x, Φ_y), where Φ is a velocity potential function, and a viscous solenoidal vector (U, V). Combining this with (3) immediately reveals that Φ is governed by Laplace's equation throughout the entire depth of the fluid:

$$\nabla^2 \Phi = 0, \qquad -\mu_1 h \leqslant y \leqslant H. \tag{16}$$

The governing equation for the solenoidal velocity vector $\boldsymbol{U}$ is obtained from the momentum equation for the lower layer, (5), and has the form

$$\boldsymbol{U}_t - \epsilon^4 \kappa \nabla^2 \boldsymbol{U} = \epsilon(\nabla \Phi + \boldsymbol{U}) \times (\nabla \times \boldsymbol{U}), \qquad -\mu_1 h \leqslant y \leqslant 0. \tag{17}$$

From this equation, it is clear that $\boldsymbol{U}$ must have a boundary layer structure at both the bottom and the interface. Within these boundary layers, the vertical scale must be much shorter than the horizontal scale. Therefore, the following vertical coordinate may be introduced inside the boundary layers:

$$\hat{y} = \frac{y}{\epsilon^2}$$

This implies, with the help of continuity, that $V/U = O(\epsilon^2)$.

Turning to the boundary conditions, the free-surface kinematic and dynamic boundary conditions (6), (7) may be combined to eliminate ξ and a Taylor series expansion around $y = H$ is used to arrive at

$$\Phi_{tt} + \Phi_y = \epsilon\{-(\nabla\Phi \cdot \nabla\Phi)_t + [(\Phi_y + \Phi_{tt})\Phi_t]_y\} + O(\epsilon^2), \qquad y = H. \tag{18}$$

The bottom boundary conditions are rewritten as

$$\Phi_y = O(\epsilon^2), \qquad y = -\mu_1 h, \tag{19}$$

$$\Phi_x + U = 0, \qquad y = -\mu_1 h. \tag{20}$$

Finally, the interfacial boundary conditions (10), (11) and (12) may be combined in order to eliminate η. Using a Taylor series expansion about $y = 0$, the kinematic conditions combined yield

$$\Phi_y^- - \Phi_y^+ = \epsilon\left\{\frac{1}{1-\gamma}(\Phi_x^- + U^- - \Phi_x^+)(\gamma\Phi_{tx}^+ - \Phi_{tx}^-) - \frac{1}{1-\gamma}(\Phi_{yy}^- - \Phi_{yy}^+)(\gamma\Phi_t^+ - \Phi_t^-)\right\} + O(\epsilon^2), \qquad y = 0. \tag{21}$$

Recall that the + and − superscripts denote evaluation just above and below the linearized interface $y = 0$.

Similarly, manipulation of the dynamic condition yields

$$(\Phi_{tt}^- + \Phi_y^-) - \gamma(\Phi_{tt}^+ + \Phi_y^+) = \epsilon\{-(\nabla\Phi^- \cdot \nabla\Phi^-)_t + \gamma(\nabla\Phi^+ \cdot \nabla\Phi^+)_t + \frac{1}{1-\gamma}(\gamma\Phi_t^+ - \Phi_t^-)(\gamma\Phi_{tty}^+ + \gamma\Phi_{yy}^+ - \Phi_{tty}^- - \Phi_{yy}^-) - (\Phi_x^- + \tfrac{1}{2}(U^-)^2)_t - U^-\Phi_{xt}^-\}, \qquad y = 0. \tag{22}$$

And finally, revisiting the interfacial shear condition yields

$$2\Phi_{xy}^- + U_y^- = O(\epsilon), \qquad y = 0. \tag{23}$$

4.1. *The inviscid limit*

The problem is greatly simplified if both layers are assumed to be inviscid. In this case, the solenoidal contribution to the velocity vector disappears. The velocity potential Φ is then expanded as

$$\Phi = \phi e^{i(x-\omega t)} + \epsilon\{\psi e^{i(x/\mu_1+\sigma_1 t)} + \chi e^{i(x/\mu_2-\sigma_2 t)} + q(\phi,\phi)\} + \epsilon^2\{\ldots + \psi' e^{i(x/\mu_1+\sigma_1 t)} + \chi' e^{i(x/\mu_2-\sigma_2 t)} + \ldots\} + \text{c.c.} \tag{24}$$

In this expansion, the first three terms are the linear harmonics describing the interacting wave triad. Recalling that the analysis is restricted to the case of small internal waves only, the internal wave harmonics appear at $O(\epsilon)$ and not at $O(1)$. The fourth term represents the forced motion due to self-interaction of the surface wave. Terms in the second bracket are forced harmonics due to interactions between the surface wave and the internal waves, and c.c. denotes the complex conjugate. To clarify what is meant by a forced harmonic, note for example that the product of $\phi e^{i(x-\omega t)}$ and $\psi e^{i(x/\mu_1+\sigma_1 t)}$ yields, with the help of (1) and (2), a term that is in phase with $\chi e^{i(x/\mu_2-\sigma_2 t)}$. Such terms will then provide boundary forcing in the inhomogeneous boundary value problem for χ'.

4.1.1. *Linear harmonics*

The linear harmonics all satisfy Laplace's equation (16) and the linear versions of the boundary conditions (18), (19), (21), and (22). A slow time scale is introduced, defined by $t_1 = \epsilon t$. Recall that the internal wave amplitudes are taken to be functions of this slow time scale. For the surface wave, the solution is given by

$$\phi = \frac{-\mathrm{i}}{\omega \cosh(H)} \cosh(y) + O(\mu_1 h), \qquad 0 \leqslant y \leqslant H,$$

$$\phi = \frac{-\mathrm{i}\gamma}{\omega \cosh(H)} \cosh(y) + O(\mu_1 h), \qquad -\mu_1 h \leqslant y \leqslant 0.$$

with the accompanying dispersion relationship given by

$$\omega^2 = \tanh(H) + O(\mu_1 h).$$

The solution for the left-travelling internal wave perturbation ψ is given by

$$\psi = -\mathrm{i}\mu_1 \sigma_1 a_1 \mathrm{e}^{-y/\mu_1} + O(\mathrm{e}^{-H/\mu_1}), \qquad 0 \leqslant y \leqslant H,$$

$$\psi = \frac{\mathrm{i}\mu_1 \sigma_1 a_1}{\sinh(h)} \cosh\left(\frac{y}{\mu_1} + h\right) + O(\mathrm{e}^{-H/\mu_1}), \qquad -\mu_1 h \leqslant y \leqslant 0,$$

where the $O(\mathrm{e}^{-H/\mu_1})$ terms arise from the free-surface boundary condition. The dispersion relationship is given by

$$\sigma_1^2 = \frac{1-\gamma}{\mu_1(\gamma + \coth(h))} + O(\mu_1 h).$$

Note that $1-\gamma$ is necessarily the same order as μ_1. This reveals that subharmonic behaviour is not possible in strongly stratified systems.

Finally, for the right-travelling internal wave χ, the solution is given as

$$\chi = \mathrm{i}\mu_2 \sigma_2 a_2 \mathrm{e}^{-y/\mu_2} + O(\mathrm{e}^{-H/\mu_2}), \qquad 0 \leqslant y \leqslant H,$$

$$\chi = \frac{-\mathrm{i}\mu_2 \sigma_2 a_2}{\sinh(\mu_1 h/\mu_2)} \cosh\left(\frac{y+\mu_1 h}{\mu_2}\right) + O(\mathrm{e}^{-H/\mu_2}), \qquad -\mu_1 h \leqslant y \leqslant 0,$$

with the dispersion relationship

$$\sigma_2^2 = \frac{1-\gamma}{\mu_2(\gamma + \coth(\mu_1 h/\mu_2))} + O(\mu_1 h).$$

4.1.2. *Forced harmonics and the solvability condition*

At the second order, $O(\epsilon^2)$, quadratic interactions between the above linear harmonics give rise to secular term forcing on the right-hand sides of the nonlinear boundary conditions (18), (21), and (22). Since the homogeneous version of the boundary value problem had a non-trivial solution, the inhomogeneous problem has a solution only if the forcing terms are orthogonal to the homogeneous solution. This orthogonality can be expressed in the form of an application of Green's theorem and will result in the desired evolution equations for the internal wave amplitudes.

For example, to solve for χ', which represents the forced second-order harmonic in phase with the right-travelling internal wave, (24) is substituted into the governing equation and boundary conditions. Then, terms proportional to ϵ^2 and $\mathrm{e}^{\mathrm{i}(x/\mu_2 - \sigma_2 t)}$ are collected to yield the inhomogeneous problem. Applying Green's theorem to χ' and χ

across the depths of both layers yields

$$\int_0^H (\chi\chi'_{yy} - \chi'\chi_{yy})\mathrm{d}y = [\chi\chi'_y - \chi'\chi_y]_0^H, \tag{25}$$

$$\int_{-\mu_1 h}^0 (\chi\chi'_{yy} - \chi'\chi_{yy})\mathrm{d}y = [\chi\chi'_y - \chi'\chi_y]_{-\mu_1 h}^0. \tag{26}$$

With manipulation, these equations lead to the following evolution equation:

$$\frac{\mathrm{d}a_2}{\mathrm{d}t_1} = \mathrm{i}\alpha_2 a_1, \tag{27}$$

$$\alpha_2 = \frac{1}{2(1-\gamma)\omega\cosh(H)}[2\gamma\sigma_1\sigma_2(1+\coth(h)) + (1-\sigma_2^2\mu_2\coth(\mu_1 h/\mu_2))(\gamma-1)(1/\mu_1)].$$

Repeating this process for the other internal forced harmonic, ψ', yields the second evolution equation

$$\frac{\mathrm{d}a_1}{\mathrm{d}t_1} = \mathrm{i}\alpha_1 a_2, \tag{28}$$

$$\alpha_1 = \frac{1}{2(1-\gamma)\omega\cosh(H)}[2\gamma\sigma_2\sigma_1(1+\coth(\mu_1 h/\mu_2)) + (1-\sigma_1^2\mu_1\coth(h))(\gamma-1)(1/\mu_2)].$$

Cross-differentiation of (27) and (28) yields the solutions for the internal wave amplitudes.

$$a_1, a_2 \propto \mathrm{e}^{\pm(-\alpha_1\alpha_2)^{1/2}t_1}. \tag{29}$$

Recalling that $\sigma_1 \approx \sigma_2$ and $\mu_1 \approx \mu_2$, it is clear that the interaction coefficients α_1 and α_2 are of the same sign. Therefore, the growth rate in this inviscid solution is purely imaginary. As a result, the solution predicts that the amplitudes of the perturbation internal waves will modulate slowly with time but will not exhibit instability in the form of exponential growth. The conclusion is that the internal wave is marginally stable in the inviscid case.

4.2. *Viscous interaction*

By introducing viscosity and a non-zero solenoidal velocity in the lower layer, the forcing on the right-hand side of the interfacial boundary conditions (21), (22) contains terms not present in the inviscid formulation. This results in modified evolution equations for the amplitudes of the internal waves. In this section, leading-order modifications due to viscosity are introduced to the interaction formulation described in the previous section.

As before, a velocity potential Φ exists in both layers, as expanded in (24). The three linear harmonics have the same solutions and dispersion relationships as found in the inviscid formulation. In the lower layer however, in addition to the irrotational velocity vector, there now exists the solenoidal velocity vector $\boldsymbol{U}$. There are two boundary layers to solve for in the lower layer: one at the interface and one at the bottom. In general, both the horizontal and vertical components of the solenoidal velocity vector can contribute to the boundary forcing. However, based on the

assumption of weak viscosity, it was shown that $V = O(\epsilon^2)U$. As a result, solutions for the vertical components need not be pursued at this order of analysis. With this, the solution for the bottom boundary layer can be neglected entirely, as it is V and not U which yields corrections to the bottom boundary condition and, ultimately, the evolution equations. The effects of stronger viscosity will be presented in future work.

To solve for U, a form consistent with the linear wave triad is adopted:

$$U = U_0(y)e^{i(x-\omega t)} + \epsilon\{U_1(y)e^{i(x/\mu_1+\sigma_1 t)} + U_2(y)e^{i(x/\mu_2-\sigma_2 t)}\} + \text{c.c.} \tag{30}$$

Substituting (30) into the leading-order forms of (23) and (17) and assuming that U goes to zero as $\hat{y} \to -\infty$, it is easily shown that

$$\left.\begin{aligned} U_0 &= 0, \\ U_1 &= (1-i)\frac{\epsilon^2}{\mu_1}\sigma_1 a_1\left(\frac{2\kappa'}{\sigma_1}\right)^{1/2}\exp\left[(1+i)\left(\frac{\sigma_1}{2\kappa'}\right)^{1/2}\hat{y}\right], \\ U_2 &= -(1+i)\frac{\epsilon^2}{\mu_2}\sigma_2 a_2\left(\frac{2\kappa'}{\sigma_2}\right)^{1/2}\exp\left[(1-i)\left(\frac{\sigma_2}{2\kappa'}\right)^{1/2}\hat{y}\right]. \end{aligned}\right\} \tag{31}$$

Having obtained U, solution of the inhomogeneous problem for the forced harmonics may be repeated. Reapplying Green's theorem to χ' and χ across both of the fluid layers yields the viscosity-modified evolution equation for a_2

$$\frac{da_2}{dt_1} = i\alpha_2' a_1, \tag{32}$$

$$\alpha_2' = \alpha_2 + \frac{\gamma(2\omega-\sigma_1)\epsilon^2(1-i)}{\omega\cosh(H)\mu_1(1-\gamma)}\left(\frac{\kappa'\sigma_1}{2}\right)^{1/2}.$$

Repeating the analysis for the other harmonic ψ' leads to the companion modified evolution equation

$$\frac{da_1}{dt_1} = i\alpha_1' a_2, \tag{33}$$

$$\alpha_1' = \alpha_1 + \frac{\gamma(2\omega-\sigma_2)\epsilon^2(1+i)}{\omega\cosh(H)\mu_2(1-\gamma)}\left(\frac{\kappa'\sigma_2}{2}\right)^{1/2}.$$

As before, cross-differentiation between the two evolution equations leads to the solutions for the internal wave amplitudes.

$$a_1, a_2 \propto e^{\pm(-\alpha_1'\alpha_2')^{1/2}t_1}. \tag{34}$$

Clearly, the coefficients of the interaction equations have been modified by the inclusion of viscosity so that they are now both complex. The result of this is that the growth rates are now complex, unlike the inviscid case in which they were found to be purely imaginary. The real part of the growth rates leads to exponential growth of the internal waves. Physically, the effect of the viscosity is to adjust the phase of the pressure at the interface. As a result, the interfacial pressure and normal velocity are no longer 90° out of phase, and there is work done on the internal waves, leading to physical growth of their amplitudes. Having completed the formulation and solution, attention is now given to the quantitative and qualitative nature of the results.

4.3. *Theoretical results and discussion*

As already mentioned, the imaginary part of the growth rates modulates the frequency of the internal waves and the real part describes the exponential growth of their

amplitudes. Both the growth rate and the modulation are functions of $H, h, \omega, \kappa', \epsilon$, and γ. As the primary emphasis of this study has been on quantifying the physical growth of the internal waves, the dependence of the frequency modulation on the various parameters is not discussed except to note that the inclusion of viscosity reduces the amount of modulation.

To be consistent with the formulation, the results are presented in a non-dimensional format. Furthermore, note that the growth rates have been converted back to the fast time scale. To aid in the physical interpretation of the results, one set of computations for dimensional parameters is considered before turning to the non-dimensional results. The following input values were specified: $H = 5$ m, $h = 0.5$ m, $\omega = 1\text{rad s}^{-1}$, $A = 0.5$ m, $\nu' = 10^{-2}\text{m}^2\,\text{s}^{-1}$, $\gamma = 0.95$. The corresponding non-dimensional parameters are given by: $H = 0.781, h = 0.637, \omega = 0.808, \sigma_1 = 0.387, \sigma_2 = 0.421, \mu_1 = 0.123, \mu_2 = 0.109, \epsilon = 0.078, \kappa' = 5.30$. The associated e-folding time constant of the internal waves is found to be 316 s. With these dimensional results as an example, attention is turned to the variation of the non-dimensional growth rates with each of the non-dimensional input parameters.

Recall that for the inviscid case, the growth rates were found to be purely imaginary, so that the amplitudes did not exhibit exponential growth. The effect of the lower-layer viscosity on the growth rate of the internal waves is illustrated in figure 5(*a*). Clearly, the growth rate is an increasing function of viscosity. Note as well that in the asymptotic case of zero viscosity, the growth rate approaches zero, recovering the results of the inviscid limit.

Figure 5(*b*) demonstrates that the growth rates are decreasing functions of the upper-layer depth. This result makes clear physical sense because as the upper layer becomes large with respect to the surface wavelength, the effects of the free surface, and therefore the pressure and velocity forcing, are substantially diminished at the interface. Figure 5(*c*) indicates a similar behaviour of the growth rates with respect to the lower-layer depth. An interesting difference, however, is that as the lower layer becomes deep, the growth rates asymptote to a finite value, rather than to zero as was the case for the upper-layer depth. This suggests that the analysis may find an application to thermocline dynamics, where a finite upper layer overlies a very deep lower layer.

The effect of the density ratio on the growth rates is illustrated in figure 5(*d*) As shown, weakly stratified systems are significantly more unstable than moderately stratified systems. This clearly agrees with the physical intuition that a strong density gradient in a stratified system is stabilizing.

Finally, the steepness of the surface wave is an extremely important parameter, as is expected since it served as the parameter of expansion. As demonstrated in figure 5(*e*), the effect of increasing steepness is to increase the growth rates. This result as well is consistent with physical intuition which suggests that as the surface wave climate becomes more severe, the excitation of internal waves will be enhanced. Finally, the effect of the surface wave frequency was found to be slight and is not shown.

4.4. *Concluding remarks*

A second-order multiple-time-scaling analysis has been used to describe the interaction between a progressive surface wave and a nearly standing subharmonic internal wave in a two-layer fluid system. When the wave triad satisfied certain resonance conditions, the amplitudes of the internal waves were shown to evolve as complex exponentials. This complex exponential, which describes both the growth rate and the frequency

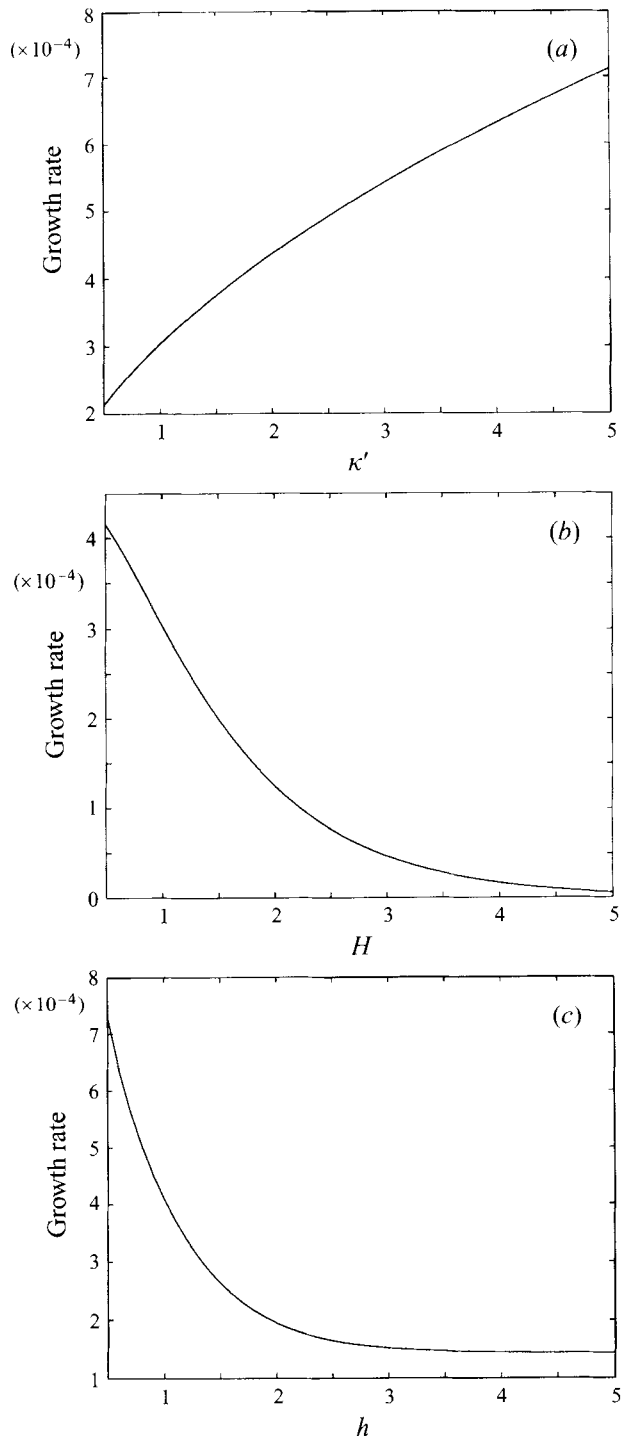

FIGURE 5(*a–c*). For caption see facing page.

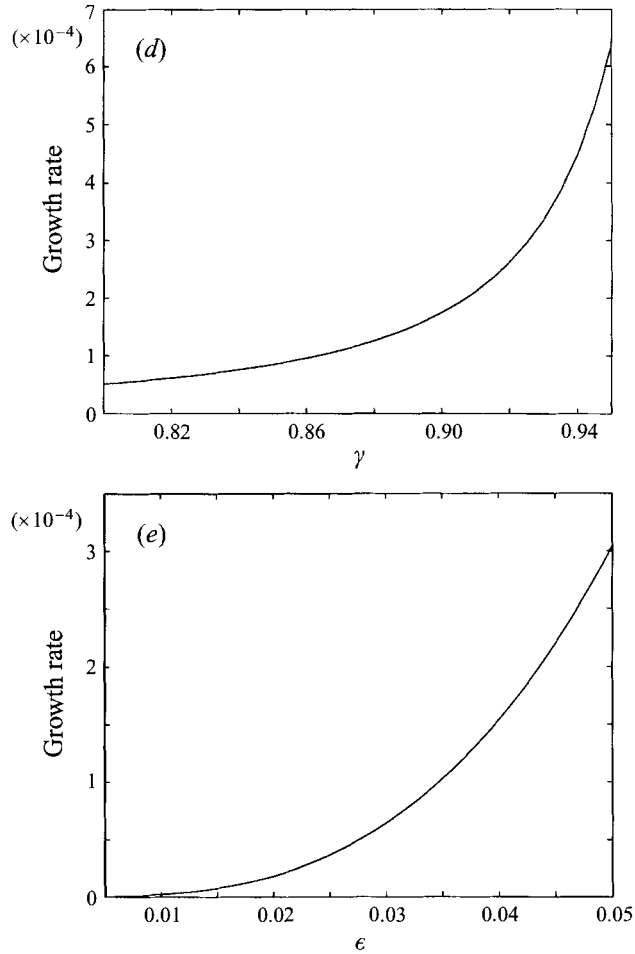

FIGURE 5. Growth rate variation with (*a*) κ': $H = 1, h = 1, \omega = 1, \epsilon = 0.05, \gamma = 0.95$. (*b*) H: $\kappa' = 1, h = 1, \omega = 1, \epsilon = 0.05, \gamma = 0.95$. (*c*) h: $H = 1, \kappa' = 1, \omega = 1, \epsilon = 0.05, \gamma = 0.95$. (*d*) γ: $H = 1, h = 1, \omega = 1, \epsilon = 0.05, \kappa' = 1$. (*e*) ϵ: $H = 1, h = 1, \omega = 1, \kappa' = 1, \gamma = 0.95$.

modulation of the internal waves, was found to be a function of the fluid layer depths, density ratio, and the surface wave conditions. Additionally, the effects of viscosity were included for the first time in the interaction problem, and the destabilizing effect of viscosity emerged as a remarkable result. Physically, the interfacial pressure and normal velocity were found to be 90° out of phase in the inviscid case, yielding no net work done on the internal waves. The inclusion of viscosity in the lower layer adjusted the phase of the pressure so that work could be done at the interface.

The generality of the analysis lends itself to widespread application. In estuarine environments, stratified systems consisting of fresh water overlying salt water or water overlying a suspended sediment layer frequently occur. In both situations, excitation of internal waves contributes significantly to mixing and water quality and in the latter case internal waves contribute to enhancement of suspension and transport of sediment and pollutants trapped in sediment beds.

In closing, it is worth noting that the present analysis is sufficient to predict an initial instability only. Clearly, the exponential growth cannot describe the steady

state evolution of the internal waves, or the resonance of three waves of comparable amplitude. It is anticipated that by extending the analysis to the next order, and allowing for finite internal waves, a governing equation describing the steady state amplitudes of the internal waves can be obtained.

This work was supported in part by grants from the National Science Foundation (grant CTS-9215889) and the Environmental Protection Agency (grant R817170020). The authors would like to thank Dr Feng Wen, Chi-Ming Huang, and Rachel Kamman for their assistance in obtaining the experimental results. D. F. Hill would also like to acknowledge support from the National Defense Science and Engineering Graduate Fellowship.

REFERENCES

BALL, K. 1964 Energy transfer between external and internal gravity waves. *J. Fluid Mech.* **19**, 465–478.

BREKHOVSKIKH, L. M., GONCHAROV, V. V., KURTIPOV, V. M. & NANGOL'NYKH, K. A. 1972 Resonant excitation of internal waves by nonlinear interaction of surface waves. *Izv. Akad. Nauk SSSR, Fiz-Atmos. Okeana* **8**, 192–203. (English Transl. *Atmos. Ocean. Phys.* **8**, 192–197.)

FODA, M. A. & TZANG, S. Y. 1994 Resonant fluidization of silty soil by water waves. *J. Geophys. Res.* **99** (C10), 20463–20475.

SIMMONS, W. F. 1969 A variational method for weak resonant wave interactions. *Proc. R. Soc. Lond.* A **309**, 551–575.

THORPE, S. A. 1968 On standing internal gravity waves of finite amplitude. *J. Fluid Mech.* **24**, 737–751.

TING, C. K. F. & RAICHLEN, F. 1986 Wave interaction with a rectangular trench. *J. Waterway, Port, Coastal, and Ocean Engng ASCE* **112** (3), 454–460.